# Band-gap widening in heavily Sn-doped $In_2O_3$

I. Hamberg and C. G. Granqvist
*Physics Department, Chalmers University of Technology, S-412 96 Göteborg, Sweden*

K.-F. Berggren, B. E. Sernelius, and L. Engström
*Theoretical Physics Group, Department of Physics and Measurement Technology, Linköping University, S-581 83 Linköping, Sweden*

(Received 17 April 1984)

Films of pure and Sn-doped semiconducting $In_2O_3$ were prepared by reactive *e*-beam evaporation. The spectral absorption coefficient was evaluated by spectrophotometry in the (2—6)-eV range. The extracted band gap increases with electron density ($n_e$) approximately as $n_e^{2/3}$ for $n_e \lesssim 10^{21}$ cm$^{-3}$. This result is interpreted within an effective-mass model for *n*-doped semiconductors well above the Mott critical density. Because of the high degree of doping, the impurities are ionized and the associated electrons occupy the bottom of the conduction band in the form of an electron gas. The model accounts for a Burstein-Moss shift as well as electron-electron and electron-impurity scattering treated in the random-phase approximation. Experiments and theory were reconciled by assuming a parabolic valence band with an effective mass $\sim 0.6m$. Earlier work on doped oxide semiconductors are assessed in the light of the present results.

## I. INTRODUCTION AND SUMMARY

In this paper we investigate the optical properties of evaporated films of doped semiconducting $In_2O_3$ in the (2—6)-eV range, i.e., around the fundamental band gap. The study serves two main purposes: to elucidate basic properties of a heavily *n*-doped semiconductor, and to improve our understanding of a technologically important material which is widely used when transmittance of visible or solar radiation needs to be combined with good electrical conduction or low thermal emittance.

We are interested in semiconductors which are *n* doped so that the Mott critical density is exceeded and for which electrons occupy the host conduction band in the form of an electron gas. The energy gap is shifted as a result of the doping. The magnitude of the shift is determined by two competing mechanisms. There is a band-gap *narrowing* which is a consequence[1,2] of many-body effects on the conduction and valence bands. This shrinkage is counteracted by the Burstein-Moss effect[3] which gives a band-gap *widening* as a result of the blocking of the lowest states in the conduction band. For doped $In_2O_3$, the net effect is to *increase* the gap.

We report below in Sec. II on the production and analysis of evaporated $In_2O_3$ films with up to 9 mol% $SnO_2$. The spectral absorption coefficient is evaluated for films with electron densities up to $\sim 10^{21}$ cm$^3$; the data indicate a band-gap widening by as much as $\sim 0.8$ eV. To understand this widening from basic principles, we outline in Sec. III a theory which includes the Burstein-Moss shift *and* self-energies due to electron-electron and electron-impurity scattering. The calculations are performed within the framework of the random-phase approximation (RPA), along the lines given in an earlier paper.[2]

A proper comparison of theory and experiments must account for the shape of the spectral absorption coefficient around the energy gap. The analysis procedure is presented in Sec. IV. We are able to reconcile theory and experiments by having effective electron masses of $\sim 0.3m$ for the conduction band and $\sim 0.6m$ for the valence band (where $m$ is the free-electron mass). Our techniques for evaluating and interpreting the band gaps go beyond what is normally done for oxide semiconductors. Hence it is of interest to consider the earlier work in the light of the present results. This is done for $In_2O_3$, CdO, and $SnO_2$ in Sec. V. As far as we know, all earlier work on these materials have neglected the self-energies. It is demonstrated that this may lead to a qualitatively incorrect interpretation of the shifted band gaps.

The present analysis provides a consistent model for the optical properties of doped $In_2O_3$ around its fundamental band gap. It embraces a doping of a host semiconductor to achieve a high density of electrons—described within the RPA—and accounts for the ensuing ionized impurities. It is gratifying that the same model can be used[4,5] for the optical performance in the infrared, where the properties are governed by a degenerate electron gas with a plasma energy $\sim 1$ eV for the highest doping levels. We are thus establishing a model capable of explaining the key properties of transparent conductors and transparent heat mirrors: a high transmittance between a properly shifted and broadened energy gap and the plasma wavelength, and a high reflectance and concomitant high conductivity beyond the plasma wavelength. Coatings with these properties, applied to substrates of glass and plastic, are extensively used for a large number of applications;[6—8] some of the most important are front-surface electrodes on solar cells and display devices, and low-emittance coatings for windows.

 

## II. FILM FABRICATION AND OPTICAL DATA

The thin films studied in this work were produced by reactive *e*-beam evaporation of pure $In_2O_3$ and of $In_2O_3$ with up to 9 mol % $SnO_2$ onto substrates of $CaF_2$ in a system with accurate process controls.[9] The deposition materials were hot-pressed pellets with 99.99% purity supplied by Kyodo International, Japan. The evaporation rate was kept at a constant value in the 0.2—0.3 nm/s interval by using the output from a vibrating quartz microbalance to feedback control the electrical power of the *e*-beam source. A constant oxygen pressure in the $(5-8)\times10^{-4}$-Torr range was maintained by continuous gas inlet through a precision valve. The substrate, positioned 35 cm above the source, was kept at $\sim$300 °C during the evaporation. These parameters are known[9] to yield particularly good optical performance. Film thicknesses were monitored on the vibrating quartz microbalance during the evaporation and were subsequently determined to an accuracy of, typically, $\pm2$ nm by a combination of optical interference methods. The analyzed films were between 75 and 1200 nm thick.

Optical properties of the films were determined by spectrophotometry. Normal transmittance ($T$) and near-normal reflectance ($R$) were recorded at room temperature as a function of photon energy ($\hbar\omega$) on a Beckman ACTA MVII double-beam instrument interfaced to a computer. Figure 1 shows typical data; (a) refers to a 75-nm-thick film made by evaporation of pure $In_2O_3$, and (b) refers to a 110-nm-thick film made by evaporation of $In_2O_3+9$ mol % $SnO_2$. A large decrease in $T$ as the photon energy is increased signifies the band gap. Oscillations in $R$ indicate optical interference.

Spectral transmittance and reflectance data were used to compute the complex refractive index, $n+ik$, of the films by use of Fresnel's equations[10] and known properties of the $CaF_2$ substrates.[11] Spectrophotometric data were selected in such a way that the ensuing optical constants were accurate to within prescribed limits, and so that spurious solutions were avoided. It was also verified that the Kramers-Kronig relation was obeyed. These aspects, which fall outside the scope of this paper, are discussed in some detail elsewhere.[12] The optical constants $n$ and $k$ were derived at $\sim$100 equally spaced energies in the (2—6)-eV interval. Figure 2 shows smooth curves drawn through these data points for the two films reported in Fig. 1. For films of pure $In_2O_3$ (solid curves), we find that $k$ goes up rapidly at $\hbar\omega\sim3.8$ eV and that $n$ is roughly 2 with a small peak at $\hbar\omega\sim4$ eV. For Sn-doped $In_2O_3$ (dashed curves), the increase in $k$ is displaced towards higher energy and now occurs at $\hbar\omega\sim4.3$ eV; the corresponding curve of $n$ again shows a small peak at $\hbar\omega\sim4$ eV.

The absorption coefficient $\alpha$ will be analyzed in detail below. This quantity is defined by

$$\alpha=4\pi k/\lambda\ , \tag{1}$$

where $\lambda$ is the wavelength. We computed $\alpha$ at $\sim$100 equally spaced energies for each sample, and joined the in-

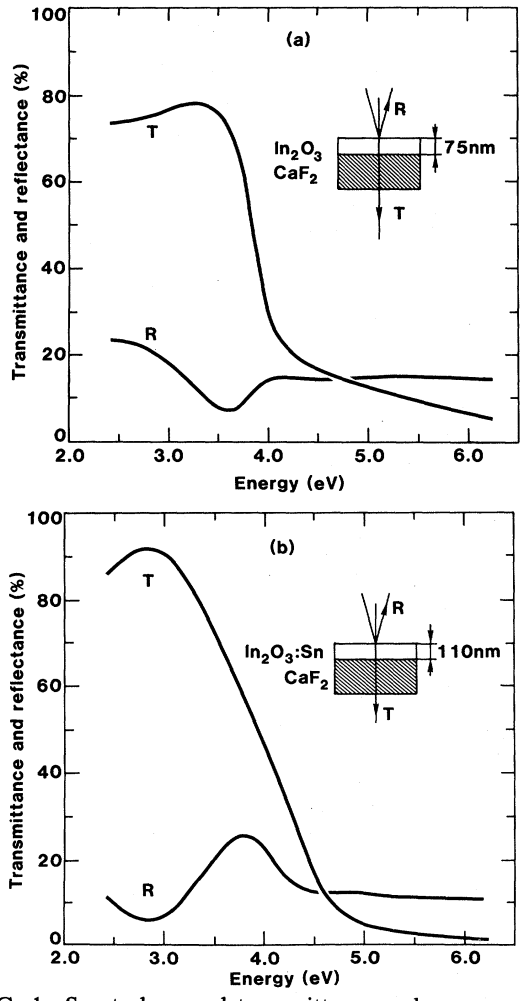


FIG. 1. Spectral normal transmittance and near-normal reflectance for films of (a) pure $In_2O_3$ and (b) Sn-doped $In_2O_3$ on substrates of $CaF_2$. Estimated experimental errors and the reproducibility among measurements on the same sample are considerably less than one percent unit.

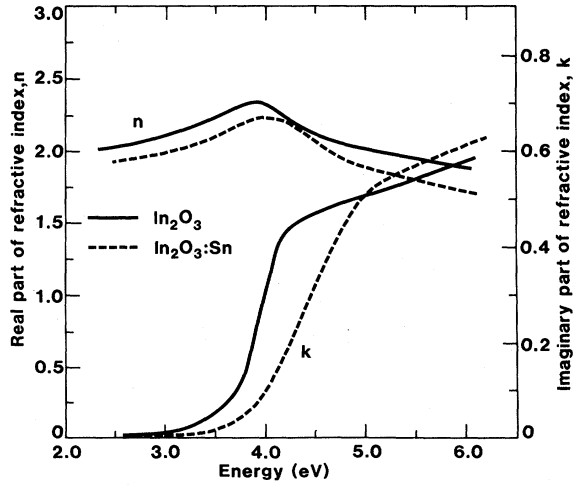


FIG. 2. Optical constants, $n$ and $k$, versus photon energy for films of pure $In_2O_3$ (solid curves) and Sn-doped $In_2O_3$ (dashed curves). Data for $n$ are less accurate than those for $k$.

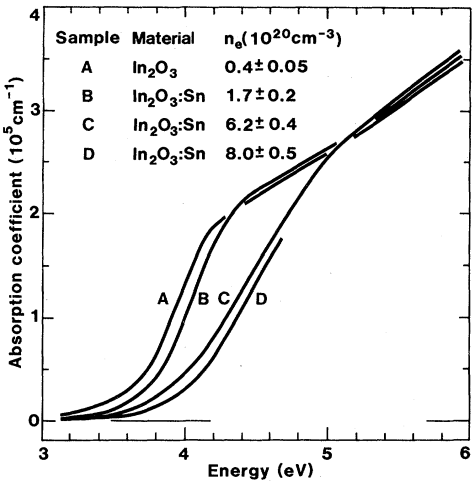


FIG. 3. Absorption coefficient versus photon energy for films of pure $In_2O_3$ and Sn-doped $In_2O_3$. Solid curves were drawn between individual data points whose scatter was less than the width of the lines. The curve denoted $D$ was obtained for a thick film which became virtually opaque for $\hbar\omega \gtrsim 4.7$ eV. Inset table shows the electron densities in the various films.

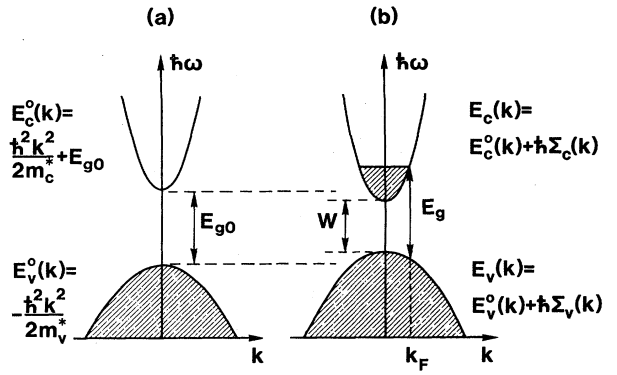


FIG. 4. (a) shows the assumed band structure of undoped $In_2O_3$ in the vicinity of the top of the valence band and the bottom of the conduction band. (b) describes the effects of Sn doping: The valence band is shifted upward by many-body effects while the conduction band is shifted downward. Shaded areas denote occupied states. Band gaps, Fermi wave number, and dispersion relations are indicated.

dividual points by smooth curves. Figure 3 shows such data for four different films. Curves $A$ and $C$ pertain to the films of pure $In_2O_3$ and Sn-doped $In_2O_3$, respectively, which were reported earlier in Figs. 1 and 2. It is apparent that the band gaps lie at different energies, and that the onset of strong absorption is rather gradual. For low energies it was found that $\ln\alpha$ versus $\hbar\omega$ displayed an approximately linear relation.[13]

The data in Fig. 3 can be systematized by considering the electron density, $n_e$, in the various films. Its magnitude was obtained from determinations of the plasma energy (i.e., the energy for which the real part of the dielectric function equals zero), as described in earlier papers.[4,5] For films of pure $In_2O_3$, we have $n_e=(0.4\pm0.05)\times10^{20}$ $cm^{-3}$ as a result of doubly charged oxygen vacancies.[14] For Sn-doped $In_2O_3$, we have electron densities between $(1.7\pm0.2)$ and $(8.0\pm0.5)\times10^{20}$ $cm^{-3}$ primarily as a consequence of the Sn atoms which enter substitutionally as $Sn^{4+}$ on $In^{3+}$ sites, and hence act as singly charged donors.[14] Actual values of $n_e$ are given in the inset of Fig. 3. It is concluded that increasing electron densities lead to a progressive enhancement of the energy gap.

## III. THEORY OF SHIFTED BAND GAPS

As a starting point for discussing the relation between optical band gap and electron density we consider the band structure of *undoped* $In_2O_3$. The band structure is unknown in most respects. The only available information concerns the direct and indirect band gaps[15] and the region around the bottom of the conduction band, which is thought to be parabolic with an effective mass ($m_c^*$) of[16] $\sim0.3m$, where $m$ is the free-electron mass. We can only make an assumption regarding the shape of the valence band; we take it to be parabolic and characterized by an effective mass ($m_v^*$) of unknown magnitude. Figure 4(a) illustrates this band structure. With the top of the valence band as reference energy, the dispersions for the unperturbed valence and conduction bands are

$$E_v^0(k)=-\hbar^2k^2/2m_v^* \tag{2}$$

and

$$E_c^0(k)=E_{g0}+\hbar^2k^2/2m_c^* , \tag{2'}$$

respectively. $E_{g0}$ is the band gap of the undoped semiconductor, $k$ is the wave number, and superscript 0 denotes unperturbed bands. Single crystalline plates of $In_2O_3$ have[15] $E_{g0}=3.75$ eV. Polycrystalline thin films may have a somewhat different $E_{g0}$; its actual magnitude is dependent on the detailed preparation conditions. A detailed discussion of these shifts is not possible, but we note that the band gap can be altered by local strain induced by impurities, point defects, and poor crystallinity.

In the *doped* material we have to consider three different effects: First, the shapes of the valence and conduction bands may not be accounted for by precisely the same effective masses as in the undoped material. Indeed, it has been found[16,17] that $m_c^*$ is weakly dependent on the electron concentration and goes up to $\gtrsim0.4m$ at $n_e\gtrsim3\times10^{20}$ $cm^{-3}$. A corresponding variation for $m_v^*$ cannot be ruled out, but nothing is known. Second, above the Mott critical density[18] the partial filling of the conduction band leads to a blocking of the lowest states and hence a widening of the optically observed band gap. This is the well-known Burstein-Moss (BM) shift.[3] Third, again above the Mott critical density the valence and conduction bands are shifted in energy as a result of electron-electron and electron-impurity scattering. In $In_2O_3$, these tend to partially compensate the BM shift. Figure 4(b) shows schematically the roles of the second and third effects.

We first neglect the role of electron-electron and electron-impurity scattering. The energy gap for direct transitions in the doped material is then given in terms of the unperturbed bands as

$$E_g^0 = E_c^0(k_F) - E_v^0(k_F) , \tag{3}$$

where $k_F = (3\pi^2 n_e)^{1/3}$ is the Fermi wave number. Alternatively, we may write

$$E_g^0 = E_{g0} + \Delta E_g^{\mathrm{BM}} , \tag{3'}$$

where the BM shift is given by

$$\Delta E_g^{\mathrm{BM}} = \frac{\hbar^2}{2m_{vc}^*}(3\pi^2 n_e)^{2/3} , \tag{4}$$

with the reduced effective mass

$$\frac{1}{m_{vc}^*} = \frac{1}{m_v^*} + \frac{1}{m_c^*} . \tag{5}$$

Equation (4) predicts an energy-gap shift proportional to $n_e^{2/3}$.

With the purpose of giving a more correct theoretical model for the shifted band gaps, we now include electron interactions and impurity scattering. The free electrons in the doped material cause a downward shift of the conduction band as a result of their mutual exchange and Coulomb interactions. This shift is further accentuated by the attractive impurity scattering. The valence band is influenced in the opposite way. The effect of the various interactions can be described simply by replacing the bare-band dispersions in Eqs. (2) and (2') by the corresponding quasiparticle dispersions

$$E_v(k,\omega) = E_v^0(k) + \hbar\Sigma_v(k,\omega) \tag{6}$$

and

$$E_c(k,\omega) = E_c^0(k) + \hbar\Sigma_c(k,\omega) , \tag{6'}$$

where $\hbar\Sigma_v$ and $\hbar\Sigma_c$ are self-energies due to electron-electron and electron-impurity scattering. We now obtain, instead of Eqs. (3) and (3'), the shifted optical gap

$$E_g = E_c(k_F,\omega) - E_v(k_F,\omega) , \tag{7}$$

or, alternatively,

$$E_g = E_{g0} + \Delta E_g , \tag{7'}$$

with

$$\Delta E_g = \Delta E_g^{\mathrm{BM}} + \hbar\Sigma_c(k_F,\omega) - \hbar\Sigma_v(k_F,\omega) . \tag{8}$$

Electron-electron (*ee*) and electron-impurity (*ei*) scattering are taken as additive processes within our perturbation treatment, i.e.,

$$\hbar\Sigma_v(k,\omega) = \hbar\Sigma_v^{ee}(k,\omega) + \hbar\Sigma_v^{ei}(k,\omega) \tag{9}$$

and

$$\hbar\Sigma_c(k,\omega) = \hbar\Sigma_c^{ee}(k,\omega) + \hbar\Sigma_c^{ei}(k,\omega) . \tag{9'}$$

We refer to Ref. 2 for details.

We first consider $\hbar\Sigma_v^{ei}$ and $\hbar\Sigma_c^{ei}$. The $Sn^{4+}$ ions—which replace substitutionally some of the $In^{3+}$ ions—act effectively as singly charged scattering centers. Their scattering potential can be written

$$V_{\mathrm{imp}}(\vec{r}) = \sum_g [V_{\mathrm{Sn}}(\vec{r} - \vec{R}_g) - V_{\mathrm{In}}(\vec{r} - \vec{R}_g)] , \tag{10}$$

where $\vec{R}_g$ runs over a random distribution of $Sn^{4+}$ on $In^{3+}$ sites. We estimate $V_{\mathrm{imp}}$ by the Heine-Abarenkov pseudopotentials[19] appropriate to the two ionic species. Figure 5 shows the Fourier transform of the unscreened difference $V_{\mathrm{Sn}}(\vec{r}) - V_{\mathrm{In}}(\vec{r})$ divided by the bare Coulomb potential $-4\pi e^2/q^2$ for a unit point charge. This ratio is close to unity for $k \lesssim 2k_F$, which is the pertinent range in the computations, thus proving that the scattering centers behave as screened point charges.[20] We stress that this simplifying feature would break down for electron concentrations much higher than those of the present films as well as for doping elements whose pseudopotentials are drastically different from that of the substituted ion. Explicit results for $\hbar\Sigma_v^{ei}$ and $\hbar\Sigma_c^{ei}$ were obtained by using $m_c^*$ from Ref. 17 (together with a reasonable extrapolation toward high electron densities). The computations of $\hbar\Sigma_v^{ee}$ and $\hbar\Sigma_c^{ee}$ require in principle that the full frequency dependence of the background is included. For simplicity we suppress this dependence. In all calculations we set the dielectric constant for the $In_2O_3$ host equal to the static value.[21]

The computations now proceed as discussed at length in Ref. 2. Thus the screening properties were included by using the random-phase approximation. As commonly done, $\hbar\omega$ in the expressions for the self-energies was put equal to $\hbar^2 k_F^2/2m_{v(c)}^*$. The interactions do not only shift the positions of the valence and conduction bands but also distort them to some degree, and hence the $k$ dependence of the self-energies should be retained in principle.

As an application of the above formulas, we now report on computed band-gap shifts versus $n_e^{2/3}$. The effective valence-band mass remains as an unknown parameter. Figure 6 contains results for three different values of $m_v^*$. It is found that an increasing electron density leads to an enhanced gap shift, and that at constant electron density the gap shift is largest for the smallest $m_v^*$.

The shifted band gap is further elucidated in Fig. 7. It shows $\Delta E_g$ for $m_v^* = 0.6m$ as well as its three contributions:

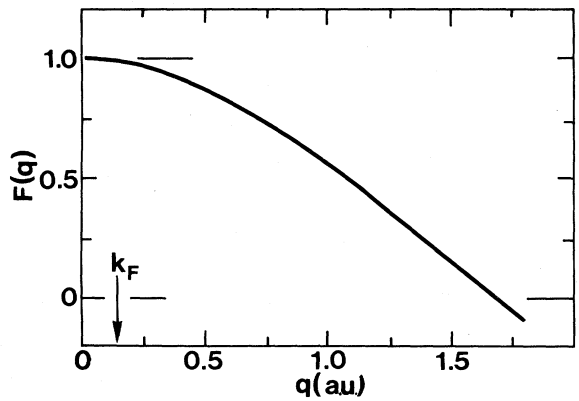


FIG. 5. $F(q)$ as a function of $q$ in atomic units (a.u.). $F(q)$ is the ratio between the Fourier transform of the bare scattering potential $V_{\mathrm{Sn}}(\vec{r}) - V_{\mathrm{In}}(\vec{r})$ and the Fourier transform of the Coulomb potential for a point charge. $F(q)$ was evaluated for $n_e = 10^{21}$ cm$^{-3}$, but is not sensitive to the electron concentration. Arrow points at $k_F$ for $n_e = 7\times 10^{20}$ cm$^{-3}$.

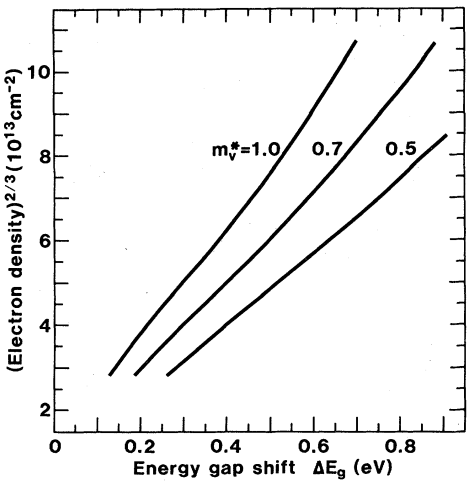


FIG. 6. $\Delta E_g$ versus $n_e^{2/3}$ computed for three magnitudes of the effective valence-band mass.

$\Delta E_g^{\mathrm{BM}}$,

$$\hbar\Sigma^{ei}(k_F)\equiv\hbar\Sigma_c^{ei}(k_F)-\hbar\Sigma_v^{ei}(k_F)\ ,$$

and

$$\hbar\Sigma^{ee}(k_F)\equiv\hbar\Sigma_c^{ee}(k_F)-\hbar\Sigma_v^{ee}(k_F)\ .$$

The BM shift is dominating except for the lowest electron concentrations. $\Delta E_g^{\mathrm{BM}}$ versus $n_e^{2/3}$ does not give a straight line, which is a consequence of the empirical relation[17] between $m_c^*$ and $n_e$ [and (Ref. 21) between the static dielectric constant and $n_e$]. The self-energies are seen to vary approximately as $n_e^{2/3}$; this dependence is rather fortuitous and is the net result of several competing effects.

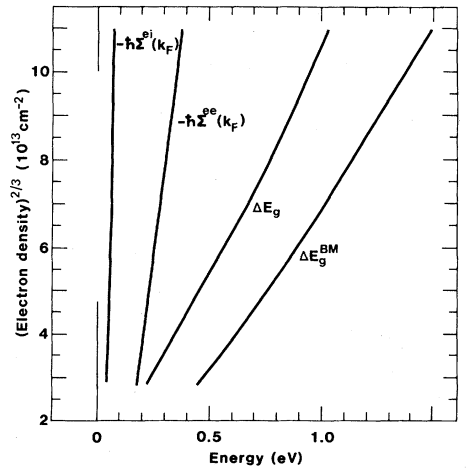


FIG. 7. $\Delta E_g$ versus $n_e^{2/3}$ computed for $m_v^*=0.6m$, and analogous plots for the contributions to $\Delta E_g$ from the Burstein-Moss shift ($\Delta E_g^{\mathrm{BM}}$), electron-impurity scattering [$\hbar\Sigma^{ei}(k_F)$], and electron-electron scattering [$\hbar\Sigma^{ee}(k_F)$].

## IV. COMPARISON OF THEORY AND EXPERIMENTS

The experimental data on $\alpha$ versus $\hbar\omega$ show a gradual onset of strong absorption, and hence it is not obvious how to locate a unique optical band gap which can be compared with $E_g$ as derived in the preceding section. In order to understand the experimental broadening, we consider the quantum-mechanical transition rate $R$ for transitions between an initial ($i$) and a final ($f$) state. According to time-dependent perturbation theory,[22] we have

$$R=\frac{2}{\hbar^2}\sum_{i,f}|\langle i|V|f\rangle|^2\frac{\tau^{-1}}{(\omega-\omega_{if})^2+\tau^{-2}}(P_i-P_f)\ , \tag{11}$$

where $\tau$ accounts for the broadening of the initial and final states, $P$ is the probability that the state is occupied, and $\omega_{fi}\equiv(E_f-E_i)/\hbar$. In the limit $\tau\to\infty$ Eq. (11) goes over to the usual golden-rule expression.

We now identify the initial states with the filled valence band and the final states with the partially filled conduction band. It is straightforward to prove that

$$R\propto\int_{x_0}^{\infty}dx(x+\hbar\omega-W)^{1/2}\frac{\Gamma}{x^2+\Gamma^2}(1-P_c)\ , \tag{12}$$

where we have introduced the notation

$$x\equiv\frac{\hbar^2k^2}{2m_{vc}^*}+W-\hbar\omega\ , \tag{13}$$

$$x_0\equiv\Delta E_g^{\mathrm{BM}}+W-\hbar\omega\ , \tag{14}$$

$$\Gamma\equiv\hbar/\tau\ . \tag{15}$$

An analogous expression for $R$ has been given by Finkenrath[23] who used classical arguments. The minimum distance between the valence and conduction band in the doped material—denoted $W$ in Fig. 4(b)—is given by the approximate relation[24]

$$W\approx E_{g0}+\hbar\Sigma_c(k_F)-\hbar\Sigma_v(k_F)\ . \tag{16}$$

In writing $R$ as in Eq. (12) we have also ignored the $k$ dependence of $\Gamma$.

Thermal excitations above the Fermi energy are represented by a Fermi function according to

$$P_c=\left\{\exp\left[\left[\frac{\hbar^2k^2}{2m_c^*}-\mu\right]\frac{1}{k_BT}\right]+1\right\}^{-1}\ , \tag{17}$$

where $k_BT$ is Boltzmann's constant times the temperature, and $\mu$ is the chemical potential. At

$$k_BT\ll\hbar^2k_F^2/2m_c^*\equiv\epsilon_F$$

we have

$$\mu\approx\epsilon_F\left[1-\frac{\pi^2}{3}\left[\frac{k_BT}{2\epsilon_F}\right]^2\right]\ . \tag{18}$$

In the limit $\Gamma\to0$ and $T\to0$, Eq. (12) goes to

$$R\propto\begin{cases}(\hbar\omega-W)^{1/2} & \text{for } \hbar\omega\geq W+\Delta E_g^{\mathrm{BM}} \quad (19)\\ 0 & \text{for } \hbar\omega<W+\Delta E_g^{\mathrm{BM}}\ . \quad (19')\end{cases}$$

This relation has formal similarities to its well-known[25] counterpart for the undoped semiconductor (for which we substitute $W \to E_{g0}$ and $\Delta E_g^{BM} \to 0$). The effect of $\Gamma$ is thus to smear the sharp absorption edge inherent in Eqs. (19) and (19′).

Putting $R \propto \alpha$ (Ref. 26) gives a complete scheme for computing the spectral absorption coefficient in terms of two parameters. One of these is taken as $W+\Delta E_g^{BM}$. It gives the energy around which the transition from low to high absorption is centered. This parameter is convenient since it can be directly compared with $E_g$ as computed in the preceding section. The second parameter is $\Gamma$, which gives the width of the transition.

For qualitative purposes, and for making rough estimates of $W+\Delta E_g^{BM}$ and $\Gamma$, it may be useful to approximate Eq. (12) in the following way. For small values of $\Gamma$ the Lorentzian is a sharply peaked function. Hence, we may consider the square-root expression as slowly varying and take it outside the integral sign. In the region of the band-gap we therefore have, with $x_0$ inserted in the square root and putting $T=0$,

$$R \propto (\Delta E_g^{BM})^{1/2}\left[1-\frac{2}{\pi}\tan^{-1}\left\{\frac{W+\Delta E_g^{BM}-\hbar\omega}{\Gamma}\right\}\right], \tag{20}$$

or, to linear order,

$$R \propto 1-\frac{2}{\pi\Gamma}(W+\Delta E_g^{BM}-\hbar\omega)\ . \tag{21}$$

According to Eq. (20) the inflection point is given by $\hbar\omega_0 \equiv W+\Delta E_g^{BM}$. A numerical study of the full expression in Eq. (12) shows that this estimate is indeed good as long as $\Gamma$ is not too large. A first estimate of the absorption edge is thus found simply by locating the maximum of $d\alpha/d(\hbar\omega)$. Drawing the tangent in the linear region of the measured absorption, the intercept with the $\hbar\omega$ axis gives $W+\Delta E_g^{BM}-(\pi\Gamma/2)$, and hence a first approximate value for $\Gamma$. The numerical study of Eq. (12) shows that this construction somewhat overestimates $\Gamma$. The final values for $W+\Delta E_g^{BM}$ and $\Gamma$ should of course be determined more accurately by fitting Eq. (12) to measured quantities, as will be described shortly. Our approximate procedure yields, however, values for $W+\Delta E_g^{BM}$ and $\Gamma$ which are most useful in connection with such a fine tuning of the parameters.

Figure 8 shows comparison between theory and experiments for two of the samples, whose spectral absorption coefficients were given earlier in Fig. 3. Open and filled circles correspond to evaluations based on spectrophotometric measurements. Solid curves denote theoretical data, which have been fitted by selecting appropriate magnitudes of $W+\Delta E_g^{BM}$ and $\Gamma$. In doing this fitting we have primarily regarded the middle parts of the curves. It is seen from Fig. 8 that theory and experiments can be brought in good agreement around the steepest parts of the curves, whereas the "tails" toward high and low energy cannot be reproduced to an equal precision. One of the possible reasons for this is that we have ignored the $k$ dependence of $\Gamma$ and $\hbar\Sigma$. The dashed curves pertain to alternative values of $\Gamma$. It is apparent that the computed

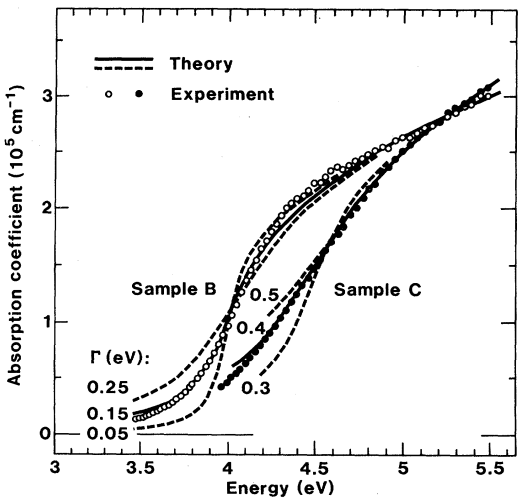


FIG. 8. Absorption coefficient versus photon energy for films of Sn-doped $In_2O_3$. Circles refer to experimental data (cf. Fig. 3). Solid and dashed curves were computed by using $W+\Delta E_g^{BM}=4.04$ and 4.46 eV for the samples, together with $\Gamma$ (in eV) as shown in the figure.

curves are strongly dependent on $\Gamma$ and, conversely, that reasonably unique $\Gamma$'s can be extracted from the experiments. When including a finite temperature we have used $T=300$ K. This parameter has a marginal influence on the curve shapes, since the degeneracy temperature of the electron gas is much higher than 300 K.

Table I contains $W+\Delta E_g^{BM}$ and $\Gamma$ as obtained from "best fits" between theory and experiments. Improved accuracy was achieved by comparing theoretical and experimental results on $d\alpha/d(\hbar\omega)$ versus $\hbar\omega$. Data for sample $D$ are less certain than for the others, since we have access to $\alpha$ only for $\hbar\omega < 4.7$ eV. It is inferred that $W+\Delta E_g^{BM}$ and $\Gamma$ both become larger as $n_e$ is increased (cf. the inset table in Fig. 3).

In Fig. 9 we compare the evaluations of $W+\Delta E_g^{BM}$ with computations of $E_g$. From Fig. 6 it is evident that the slope in the theoretical curves depends on $m_v^*$. It is then clear that $m_v^*$ should be chosen in the range $(\sim 0.6$–$0.7)m$. For $m_v^*=0.7m$ we obtain best agreement by setting $E_{g0}=3.82$ eV. For $m_v^*=0.6m$ the corresponding energy is 3.75 eV. Thus it appears that we have to assume a band gap for the undoped material which is either the same or somewhat higher than the value 3.75 eV pertaining to[15] single crystalline $In_2O_3$. An uncertainty of

TABLE I. Parameters used for fitting theoretical curves to experimental spectral absorption coefficients. The band gap corresponds to $W+\Delta E_g^{BM}$, and the width in the curve is governed by $\Gamma$.

| Sample | $W+\Delta E_g^{BM}$ (eV) | $\Gamma$ (eV) |
|---|---|---|
| *A* | 3.88 | 0.07 |
| *B* | 4.04 | 0.13 |
| *C* | 4.46 | 0.37 |
| *D* | ~4.55 | ~0.35 |

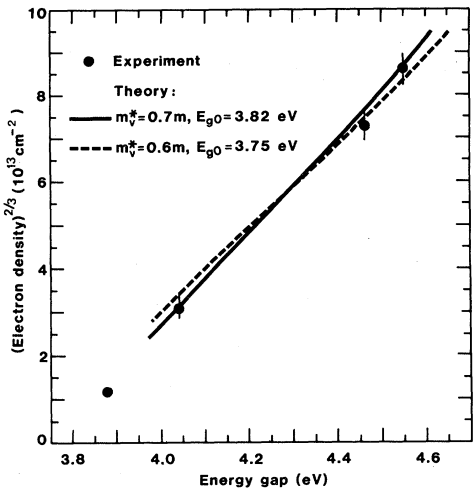


FIG. 9. Electron density to the power $\frac{2}{3}$ versus energy gap for $In_2O_3$ with different degrees of doping. Circles represent experimental data (cf. Table I). Vertical bars indicate the uncertainty in extracting $n_e$ from observed plasma frequency; they account for conceivable errors in effective conduction-band mass and dielectric constant of undoped $In_2O_3$. The uncertainty in the determination of $W+\Delta E_g^{\rm BM}$ is less easy to estimate with confidence. Solid and dashed curves indicate the results of computations using the shown values of $m_v^*$ and $E_{g0}$. Curves are confined to $n_e^{2/3}\gtrsim 3\times 10^{13}$ cm$^{-2}$ since the theory only applies to electron densities well above the Mott critical density (cf. Ref. 18).

this order of magnitude is by no means surprising. Regarding the value for $m_v^*$, there are unfortunately no band-structure calculations with which to compare.

The parameter $\Gamma$ can be understood in the following way. Because of scattering, initial and final states are collision broadened. For ionized impurity scattering one has for the conduction-band electrons

$$\frac{1}{\tau_c(k)}=\frac{2\pi}{\hbar}n_e\int\frac{d\vec{q}}{(2\pi)^3}\,|V(q)|^2\delta(E_c^0(\vec{k})-E_c^0(\vec{k}+\vec{q}))\,, \tag{22}$$

where $V(q)$ is the dielectrically screened scattering potential for a single impurity. For the valence states one finds $\tau_v^{-1}(k)=\tau_c^{-1}(k)m_v^*/m_c^*$. The electron-impurity scattering therefore gives rise to the broadening

$$\Gamma=\frac{\hbar}{\tau}=\frac{\hbar}{2}[\tau_c^{-1}(k)+\tau_v^{-1}(k)]=\frac{\hbar}{2}\tau_c^{-1}(k)(1+m_v^*/m_c^*)\,. \tag{23}$$

Putting $m_v^*=0.6m$ and $m_c^*$ as given by Ohhata *et al.*,[17] we find for $k=k_F$ that $\Gamma\approx 0.11$ eV for $n_e=1.7\times 10^{20}$ cm$^{-3}$ and $\Gamma\approx 0.17$ eV for $n_e=6.2\times 10^{20}$ cm$^{-3}$. According to Table I the experimental estimates are 0.13 and 0.37 eV, respectively. Impurity scattering thus gives the correct order of magnitude for $\Gamma$. We recall that the $k$ dependence of $\Gamma$ was neglected in Eq. (12). For this reason the agreement above may be considered as rather satisfactory.

The electron lifetime for the conduction-band electrons may also be estimated from transport measurements. The expression for this transport time $\tau_{c,\rm tr}(k)$ is the same as for $\tau_c(k)$ in Eq. (22) except for a factor $(1-\cos\theta)$, where $\theta$ is the angle between the vectors $\vec{k}$ and $\vec{k}+\vec{q}$. Since ionized impurity scattering is believed to be the most important damping mechanism, we have calculated the influence of this factor at different impurity concentrations. For low values ($\sim 10^{15}$ cm$^{-3}$) the scattering is highly anisotropic implying that $\tau_{c,\rm tr}^{-1}(k_F)\ll\tau_c^{-1}(k_F)$. Increasing the impurity concentration reduces the anisotropy so that at high doping ($\sim 10^{20}$ cm$^{-3}$) we have $\tau_{c,\rm tr}^{-1}(k_F)\lesssim\tau^{-1}(k_F)$, i.e., nearly isotropic ($s$-wave) scattering. Hence we may use $\tau_{c,\rm tr}$ to estimate the broadening $\Gamma$ by means of Eq. (23). From measurements of the frequency-dependent resistivity,[5] and hence $\tau_{c,\rm tr}$, we obtain the following $\Gamma$ values for the different samples listed in Table I: *A*, 0.05; *B*, 0.08; *C*, 0.13; *D*, 0.16 eV. Cases *B* and *C* agree quite well with our previous theoretical estimates, and as before, there is, within about a factor of two, an overall agreement with $\Gamma$ as estimated from the measured absorption coefficient. With increasing concentration there is a marked tendency of an extra contribution to $\Gamma$.

As we have demonstrated above, ionized impurity scattering is the most important contribution to $\Gamma$, but other effects may also come into play. At $T=0$ K, electron-electron interactions give no lifetime broadening at the Fermi level, but since the folding in Eq. (12) also involves states away from the Fermi energy, $\Gamma$ may be affected. Effects of electron-phonon interactions are similar. There may also be smearing effects due to local deformations of the lattice because of the randomly introduced Sn ions. The electric field of these ionized donors and the difference in atomic size of Sn relative to In affect the absolute value of the band gap for each microcell of the crystal. Hence the band gap should be statistically distributed around the value $W$. In our theoretical expressions we have taken into account the overall band-gap narrowing due to the electron-impurity and electron-electron interactions, but neglecting these possible fluctuations of the energy levels. Clearly this latter effect should increase with the doping concentration. We shall not pursue such effects or electron-electron interactions any further. For our purposes it suffices to consider ionized impurity scattering only.

## V. CRITICAL ASSESSMENT OF EARLIER WORK

Band-gap widening associated with doping has been observed in earlier work on doped $In_2O_3$ (Refs. 8, 15, 16, and 27–35), ZnO (Refs. 36 and 37), CdO (Ref. 23), $SnO_2$ (Refs. 30, and 38–43), and $Cd_2SnO_4$ (Refs. 44–46). The evaluation of shifted band gaps, as well as the interpretation of these data, are at variance with the results given above, and hence an assessment of the earlier work is appropriate.

For doped $In_2O_3$ there have been numerous[17,27,33–35] attempts to evaluate band gaps by plotting $\alpha^2$ versus $\hbar\omega$ and associating the band gap with the energy obtained through a linear extrapolation toward zero. It appears that this procedure has its root in a mistaken interpretation of Eq. (19), which would yield $W$ and not $W+\Delta E_g^{\rm BM}$. Besides

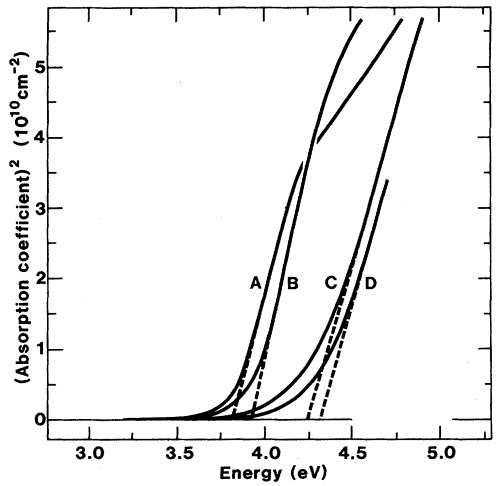


FIG. 10. Absorption coefficient squared versus photon energy for the samples $A-D$ reported earlier in Fig. 3. Dashed lines indicate linear extrapolations. The zero energy intercepts lie at 3.81, 3.91, 4.23, and 4.30 eV.

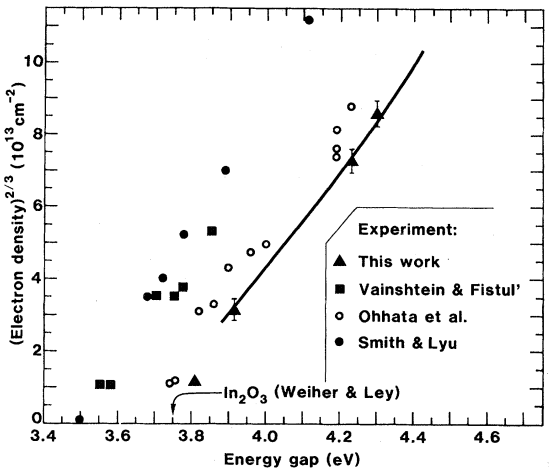


FIG. 11. Electron density to the power $\frac{2}{3}$ versus energy gap for $In_2O_3$ with different degrees of doping. Approximate energy gaps were obtained from extrapolations in plots of $\alpha^2$ versus $\hbar\omega$. Symbols denote results from the present work on pure and Sn-doped films prepared by reactive $e$-beam evaporation, as well as for sputtered films studied by Vainshtein and Fistul' (Ref. 27), Ohhata *et al.* (Ref. 17), and Smith and Lyu (Ref. 33). The electron density was determined from measurements of the Hall effect in Refs. 27 and 33, and from measurements of the plasma energy in Ref. 17. Error bars on $n_e$ are the same as those in Fig. 9. Arrow points at the energy gap for single-crystalline $In_2O_3$ as observed by Weiher and Ley (Ref. 15). Solid curve was computed from our theoretical model with $E_{g0}=3.75$ eV and $m_v^*=1.0$ m.

this, we have shown that Eq. (19) is inapplicable because of lifetime broadening effects. Nevertheless—even if a strict theoretical backing is absent—it turns out that the simple extrapolation procedure yields values which, at least for our present samples, are not grossly different from those obtained from the more elaborate analysis given in the preceding section. This point is illustrated in Fig. 10, where we replot the absorption coefficients given earlier in Fig. 3 as $\alpha^2$ versus $\hbar\omega$. The shifted band gaps, derived from the indicated extrapolations, lie below those given in Table I by a magnitude ranging from 0.07 eV for the lowest electron density to 0.25 eV for the highest electron density. We may understand this result by considering the approximate relation in Eq. (21). If squared, and if only terms up to linear order are retained, the root equals $W+\Delta E_g^{\mathrm{BM}}-\pi\Gamma/4$, i.e., the $\alpha^2$ procedure leads to band gaps which are too small by an amount $\sim\Gamma$. The values for $\Gamma$ in Table I are obviously consistent with such arguments. Other techniques to obtain shifted band gaps are based on extrapolations towards zero in plots of (Ref. 30) $\alpha$ versus $\hbar\omega$, and determinations of the energy corresponding to (Ref. 28) 10% or (Refs. 29 and 31) 50% transmittance through the samples or (Ref. 32) $\alpha=10^5$ cm$^{-1}$.

It is interesting to compare our band gaps with earlier evaluations. In order to have a consistent set of data, we focus on works in which approximate band gaps have been obtained by evaluating $\alpha^2$ versus $\hbar\omega$. Figure 11 shows a collection of such data plotted against $n_e^{2/3}$. It appears that our results (solid triangles) are in rather good agreement with those of Ohhata *et al.*[17] (open circles), whereas the results of Vainshtein and Fistul'[27] (solid squares) and of Smith and Lyu[33] (solid circles) are displaced toward lower energy. Still larger displacements have been reported by Ray *et al.*[35] We find, approximately, that the shift of the energy gap scales with $n_e^{2/3}$. This kind of relation has been reported also by others.[17,28–32,34]

The solid curve in Fig. 11 was fitted to our approximate band gaps by using the theory outlined in Sec. III. Best agreement was obtained with $m_v^*\approx 1.0$m and $E_{g0}\approx 3.75$ eV. This value of $m_v^*$ is significantly different from that found by the detailed analysis in Sec. IV, which points to the importance of using a proper evaluation of the band gap. Correspondence with the data of Ohhata *et al.*[17] could be obtained with their band gap $E_{g0}=3.67$ eV. Correspondence with the data of Vainshtein and Fistul'[27] and of Smith and Lyu[33] required $E_{g0}\approx 3.55$ eV.

The experimental observation that the band gap scales with $n_e^{2/3}$ in doped $In_2O_3$ has led to the erroneous conclusion—iterated in numerous papers[8,16,17,27–35]—that the BM shift alone would determine the band-gap widening. If, for the sake of argument, we neglect the self-energy effects, we can obtain agreement between theory and experiments only by assuming a *negative* magnitude of $m_v^*$ somewhere between $\sim -0.6$ and $\sim -1.0m$. This would imply that the valence band is curved in the same direction as the conduction band. Inclusion of the self-energies leads to a *positive* value of $m_v^*$, as discussed in Sec. IV. This proves the importance of considering electron-electron and electron-impurity scattering, and that qualitative differences can occur if they are neglected.

As far as we know, self-energy effects have been neglected in almost all[47] earlier analyses of band-gap shifts in doped oxide semiconductors. For three materials, ZnO, CdO, and $SnO_2$, there are band-structure calculations[48–50] which allow—at least in principle—an assess-

ment of the earlier analyses. $SnO_2$ doped by F and Sb has been investigated recently by Shanti *et al.*[41] Interpreting the band-gap variation as a BM shift, they concluded that $m_v^*$ would be $\sim -0.9m$. A similar analysis of CdO, performed much earlier by Finkenrath,[23] also gave a negative value of $m_v^*$. Neither of these predictions are corroborated by recent band-structure calculations for (Ref. 48) $SnO_2$ and CdO.[49] Inclusion of self-energy effects would tend to improve the correspondence between the theoretical analyses of shifted band gaps and band-structure data, but no detailed results are available at present.

## ACKNOWLEDGMENTS

This work was financially supported by grants from the Swedish Natural Science Research Council and the National Swedish Board for Technical Development.

[1]R. A. Abram, G. J. Rees, and B. L. H. Wilson, Adv. Phys. **27**, 799 (1978).

[2]K.-F. Berggren and B. E. Sernelius, Phys. Rev. B **24**, 1971 (1981).

[3]E. Burstein, Phys. Rev. **93**, 632 (1954); T. S. Moss, Proc. Phys. Soc. London Ser. B **67**, 775 (1954).

[4]I. Hamberg and C. G. Granqvist, Thin Solid Films **105**, L83 (1983).

[5]I. Hamberg and C. G. Granqvist, Proc. Soc. Photo-Opt. Instrum. Engr. **428**, 2 (1983); Appl. Phys. Lett. **44**, 721 (1984).

[6]C. G. Granqvist, Appl. Opt. **20**, 2606 (1981); Proc. Soc. Photo-Opt. Instrum. Engr. **401**, 330 (1983).

[7]H. Köstlin, in *Festköerperprobleme,* edited by P. Grösse (Vieweg, Braunschweig, 1982), Vol. 22, p. 229.

[8]K. L. Chopra, S. Major, and D. K. Pandya, Thin Solid Films **102**, 1 (1983).

[9]I. Hamberg, A. Hjortsberg, and C. G. Granqvist, Appl. Phys. Lett. **40**, 362 (1982); Proc. Soc. Photo-Opt. Instrum. Engr. **342**, 31 (1982); I. Hamberg and C. G. Granqvist, Appl. Opt. **22**, 609 (1983).

[10]M. Born and E. Wolf, *Principles of Optics,* 6th ed. (Pergamon, Oxford, 1980).

[11]Results obtained from the Harshaw Chemical Company.

[12]A. Hjortsberg, Appl. Opt. **20**, 1254 (1981); T. S. Eriksson and A. Hjortsberg, Proc. Soc. Photo-Opt. Instrum. Engr. **428**, 135 (1983).

[13]This phenomenon is known as "Urbach tails"; cf. M. V. Kurik, Phys. Status Solidi **8**, 9 (1971).

[14]G. Frank and H. Köstlin, Appl. Phys. A **27**, 197 (1982).

[15]R. L. Weiher and R. P. Ley, J. Appl. Phys. **37**, 299 (1966).

[16]Z. M. Jarzebski, Phys. Status Solidi A **71**, 13 (1982).

[17]Y. Ohhata, F. Shinoki, and S. Yoshida, Thin Solid Films **59**, 255 (1979).

[18]N. F. Mott, *Metal-Insulator Transitions* (Taylor and Francis, London, 1974). The critical density $n_c$ for the metal-insulator transition in a doped semiconductor can be estimated from Mott's criterion $n_c^{1/3}a_H \approx 0.25$. The effective Bohr radius is $a_H = \epsilon_0 \hbar^2 / m_c^* e^2$, where $\epsilon_0$ is the static dielectric constant of the host material [P. P. Edwards and M. J. Sienko, Phys. Rev. B **17**, 2575 (1978)]. For $n$-type $In_2O_3$ we thus obtain $n_c \approx 4\times 10^{18}$ cm$^{-3}$. One should recall, however, that our $e$-beam evaporated $In_2O_3$ films have $n_e \approx 4\times 10^{19}$ cm$^{-3}$ as a result of doubly charged oxygen vacancies.

[19]A. O. E. Animalu and V. Heine, Philos. Mag. **12**, 1249 (1965); M. L. Cohen and V. Heine, in *Solid State Physics,* edited by H. Ehrenreich, F. Seitz, and D. Turnbull (Academic, New York, 1970), Vol. 24.

[20]Recent calculations of the frequency-dependent resistivity also show that the impurities may be treated as point charges to a high degree of accuracy [L. Engström and I. Hamberg (unpublished)].

[21]The static dielectric constant is adequate for electron-impurity scattering; cf. B. E. Sernelius and K.-F. Berggren, Philos. Mag. **43**, 115 (1981). Similar to the case of $m_c^*$, the static dielectric constant is related to $n_e$. We use the dependence inherent in the results by Ohhata *et al.* (Ref. 17).

[22]See, for example, G. H. Wannier, *Elements of Solid State Theory* (Cambridge University Press, Cambridge, England, 1959), p. 212.

[23]H. Finkenrath, Z. Phys. **159**, 112 (1960).

[24]Equation (16) would be exact in a rigid-band model (i.e., assuming only vertical displacements of the energy bands).

[25]See, for example, F. Wooten, *Optical Properties of Solids* (Academic, New York, 1972), p. 115.

[26]In practice it makes little difference whether we equate $R$ with $\alpha$ ($\sim k/\lambda$) or $\epsilon_2\omega$ ($\sim nk/\lambda$), since $n$ is nearly constant.

[27]V. M. Vainshtein and V. I. Fistul', Fiz. Tekh. Poluprovodn. **1**, 135 (1967) [Sov. Phys.—Semicond. **1**, 104 (1976)].

[28]H. Köstlin, R. Jost, and W. Lems, Phys. Status Solidi A **29**, 87 (1975).

[29]W. G. Haines and R. H. Bube, J. Appl. Phys. **49**, 304 (1978).

[30]J.-C. Manifacier, L. Szepessy, J. F. Bresse, M. Perotin, and R. Stuck, Mater. Res. Bull. **14**, 163 (1979).

[31]A. J. Steckl and G. Mohammed, J. Appl. Phys. **51**, 3890 (1980).

[32]M. Mizuhashi, Thin Solid Films **70**, 91 (1980).

[33]F. T. J. Smith and S. L. Lyu, J. Electrochem. Soc. **128**, 2388 (1981).

[34]J. Szczyrbowski, A. Dietrich, and H. Hoffman, Phys. Status Solidi A **69**, 217 (1982); **78**, 243 (1983).

[35]S. Ray, R. Banerjee, N. Basu, A. K. Batabyal, and A. K. Barua, J. Appl. Phys. **54**, 3497 (1983).

[36]A. P. Roth, J. B. Webbs, and D. F. Williams, Solid State Commun. **39**, 1269 (1981); Phys. Rev. B **25**, 7836 (1982).

[37]O. Carporaletti, Sol. Energy Mater. **7**, 65 (1982).

[38]T. Arai, J. Phys. Soc. Jpn. **15**, 916 (1960).

[39]H. Koch, Phys. Status Solidi, **7**, 263 (1964).

[40]S. P. Lyashenko and V. K. Miloslavskii, Opt. Spektrosk. **19**, 108 (1965) [Opt. Spectrosc. (USSR) **19**, 55 (1965)].

[41]E. Shanti, A. Banerjee, V. Dutta, and K. L. Chopra, J. Appl. Phys. **51**, 6243 (1980); **53**, 1615 (1982); E. Shanti, A. Banerjee, and K. L. Chopra, Thin Solid Films **88**, 93 (1982).

[42]K. B. Sundaram and G. K. Bhagavat, J. Phys. D **14**, 921 (1981).

[43]K. Suzuki and M. Mizuhashi, Thin Solid Films **97**, 119 (1982).

[44]A. J. Nozik, Phys. Rev. B **6**, 453 (1972).

[45]N. Miyata, K. Miyake, K. Koga, and T. Fukushima, J. Electrochem. Soc. **127**, 918 (1980).

[46]E. Leja, K. Budzyńska, T. Pisarkiewicz, and T. Stapiński, Thin Solid Films **100**, 203 (1983).

[47]Work on ZnO by Roth *et al.* (Ref. 36) has considered self-energy effects.
[48]J. Robertson, J. Phys. C **12**, 4767 (1979).
[49]J. C. Boettger and A. B. Kunz, Phys. Rev. B **27**, 1359 (1983).
[50]D. M. Kolb and H. -J. Schulz, Curr. Top. Mater. Sci. **7**, 227 (1981).